Journal of Physics D: Applied Physics

TOPICAL REVIEW

Negative piezoelectricity in quasi-two/one-dimensional ferroelectrics

To cite this article: Ning Ding and Shuai Dong 2025 *J. Phys. D: Appl. Phys.* **58** 073001

IOP Publishing Journal of Physics D: Applied Physics
J. Phys. D: Appl. Phys. **58** (2025) 073001 (15pp) https://doi.org/10.1088/1361-6463/ad91c3

Topical Review

Negative piezoelectricity in quasi-two/one-dimensional ferroelectrics

Ning Ding* **and Shuai Dong***

Key Laboratory of Quantum Materials and Devices of Ministry of Education, School of Physics, Southeast University, Nanjing 21189, People's Republic of China

E-mail: dingning@seu.edu.cn and sdong@seu.edu.cn

Received 30 June 2024, revised 11 October 2024
Accepted for publication 13 November 2024
Published 4 December 2024

Abstract

In recent years, the investigation of low-dimensional ferroelectrics has attracted great attention for their promising applications in nano devices. Piezoelectricity is one of the most core properties of ferroelectric materials, which plays an essential role in micro-electromechanical systems. Very recently, anomalous negative piezoelectricity has been predicted/discovered in many quasi-two-dimensional layered ferroelectric materials. In this Topical Review, we will briefly introduce the negative piezoelectricity in quasi-two/one-dimensional ferroelectrics, including its fundamental concepts, typical materials, theoretical predictions, as well as experimental phenomena. The underlying physical mechanisms for negative piezoelectricity are divergent and vary case by case, which can be categorized into four types: first, the soft van der Waals (vdW) layer is responsible for the volume shrinking upon pressure while the electric dipoles are from the non vdW layer; second, the noncollinearity of local dipoles creates a ferrielectricity, which leads to orthogonal ferroelectric and antiferroelectric axes; third, the electric dipoles come from interlayer/interchain couplings, which can be enhanced during the volume shrinking; fourth, the special buckling structure contributes to local dipoles, which can be enhanced upon pressure. In real materials, more than one mechanism may work together. Finally, future directions of negative piezoelectricity and their potential applications are outlined.

Keywords: negative piezoelectricity, vdW materials, sliding ferroelectrics

1. Introduction

Ferroelectrics are functional materials that have spontaneous macroscopic polarization and the polarization can be reversed by an externally electric field. Due to the characteristics of non-volatility when power is turned off, and the fact that the phase transition temperature can generally reach room temperature, the study of ferroelectrics has received widespread attention [1, 2]. Over the past century, many advances have been made in ferroelectric physics and materials research. From the perspective of physical mechanism. Crystal symmetry group theory, phonon soft mode theory, and Landau phase transition theory support the framework of traditional ferroelectric physics and successfully describe a series of physical effects including ferroelectricity, piezoelectricity, and ferroelectric photovoltaic effects. From the perspective of materials, various types of ferroelectrics have been reported, including three-dimensional oxides/fluoride ferroelectrics, organic ferroelectrics and so on [3–8]. From

* Authors to whom any correspondence should be addressed.

the perspective of applications, ferroelectrics can be used in non-volatile memories, field-effect transistors, ferroelectric photovoltaic devices, sensors and so on [9–14].

The piezoelectric effect describes the linear electromechanical interaction between the mechanical and electrical states in materials without inversion symmetry, which has attracted great attention [15–18]. It is known that ferroelectrics must be piezoelectrics, but piezoelectrics are not necessarily ferroelectrics. In other words, piezoelectricity is a property associated closely with ferroelectricity. There are many applications based on piezoelectricity, including the detection/generation of sonar waves, piezoelectric motors, various sensors and so on [9, 19, 20]. The reverse piezoelectric effect illustrates the internal creation of a mechanical strain resulting from an externally electric field. The positive and negative piezoelectric effects describe the change of polarization with deformation. Specifically, the positively piezoelectric effect widely exists in traditional perovskite ferroelectrics [21], namely the dipole of the system decreases with the compressive stress, while the negative piezoelectric effect is less common and exists in certain compounds [22–25]. The piezoelectricity of ferroelectrics is interesting and requires further exploration.

1.1. Ferroelectricity in low-dimensional materials

Since the graphene was exfoliated mechanically, two-dimensional materials have also attracted great interest owing to their distinctive properties [26]. Thousands of two-dimensional materials exfoliated from van der Waals (vdW) systems beyond graphene have been reported, which were first used to study the transport and photoelectric properties [27, 28]. In addition, due to the reduction of dimension, the vdW two-dimensional materials can lose some symmetry compared with bulk structures, which may provide a potential way to design low-dimensional ferroelectrics. The rapid development of two-dimensional materials has also expanded the study of ferroelectrics to two-dimensional and even quasi-one-dimensional systems, which maintains the advantage of ferroelectrics in the post-Moore era [29–33].

Based on the characteristics of two-dimensional materials close to the surface and easy to passivate, Wu *et al* proposed to convert non-ferroelectric materials into ferroelectrics through surface functionalization [34]. Specifically, transition-metal molecular sandwich nanowires are functionalized, which break the spatial inversion symmetry and exhibit molecular reorientation in response to an external electric field. In addition, graphene modified by hydroxyl is one of the two-dimensional ferroelectrics, and the direction of polarization is controlled by that of hydroxyl molecular [35, 36]. Furthermore, more two-dimensional materials have been functionalized by various organic molecules, which is a general approach to design the two-dimensional ferroelectrics in vdW systems [37–40].

In addition to using functional molecular modification to design two-dimensional ferroelectric materials, researchers have been committed to the search and design of intrinsic two-dimensional ferroelectric materials. Shirodkar and Waghmare have observed the unstable phonon vibration modes in monolayer MoS_2, which induces the ferroelectric phase of *d*1*T*-MoS_2 [41]. Several intrinsic two-dimensional ferroelectric materials have been confirmed by experiments. In 2015, Belianinov *et al* found that the layered material $CuInP_2S_6$ holds the room-temperature ferroelectricity [42], and the effect of nanocrystal thickness on ferroelectric properties was studied [43]. In the following experiment it has been shown that ferroelectricity is also maintained even when the thickness of $CuInP_2S_6$ films is reduced to 4 nm [44]. The unusual ferroelectric properties for the uniaxial quadruple potential well have been reported [45]. In addition, Chang *et al* observed the in-plane ferroelectric polarization in monolayer SnTe [46], and the two-dimensional ferroelectricity has also been reported in other group IV monochalcogenides including GeS, GeSe, SnS and SnSe monolayers [47, 48]. In 2016, Ding *et al* predicted the out-of-plane polarization in monolayer In_2Se_3 and other III_2-VI_3 materials [49]. Soon after, the two-dimensional ferroelectricity in monolayer In_2Se_3 was confirmed by experiments [50, 51]. Recently, the single element bismuth monolayer was synthesized and confirmed as a two-dimensional ferroelectric in experiment [52]. The structure is similar to buckled black phosphorus and the origin of ferroelectricity is a combination of charge transfer and conventional atomic distortion [53]. Furthermore, many intrinsic two-dimensional and quasi-one-dimensional ferroelectrics have been predicted theoretically [54–61].

The concept of sliding ferroelectricity was proposed by Li and Wu in 2017 [62]; it indicates that the unique stacking modes among the layers can break the spatial inversion symmetry and induce the out-of-plane polarization, which can be reversed by interlayer sliding. This discovery extends the study of two-dimensional ferroelectrics from a few specific materials to most of the currently known two-dimensional materials. Soon after, the sliding ferroelectricity in bilayer BN has been verified by experiments [63, 64]. More and more interlayer sliding ferroelectrics have been predicted and confirmed [65–85]. The layer group of possible bilayer stacking ferroelectrics and the rules for the creation and annihilation of symmetry operations can be listed by performing group theory analysis [86].

1.2. Negative piezoelectricity

Research on piezoelectricity has a 100-year history, demonstrating that materials expand from conventional bulk materials to low-dimensional systems. Piezoelectric properties differ slightly in the previous two kinds of materials. First, the traditional bulk materials including perovskite oxide and fluoride are mainly connected through ionic or covalent bonds, which are ‘hard’, while the layers/chains in most low-dimensional systems are bonded by the weak vdW interaction, which are ‘soft’. The difference in structure can strongly affect the change in polarization due to structural relaxation in response to strain, namely the internal-strain term. This may result in the ubiquity of negative piezoelectricity in layered ferroelectric materials [87]. Second, piezoelectricity

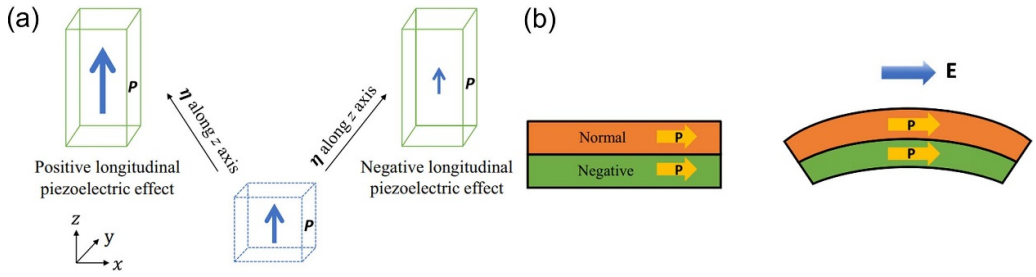

Figure 1. (a) Draft of positive and negative piezoelectricity. Assuming the z-axis is the direction of exterial strain. (b) Draft of heterostructure constructed by positive and negative piezoelectric layers. Reprinted (figure) with permission from [93], Copyright (2023) by the American Physical Society.

in low-dimensional materials exhibits strong anisotropy due to the reduced dimensionality [88–90]. Third, morphotropic phase boundary (MPB) has been widely used to explain the giant piezoelectricity in conventional bulk materials, while MPB in low-dimensional systems has received very little attention, perhaps due to challenges in achieving phase coexistence and possible polarization rotation [48, 91, 92].

Piezoelectricity is usually estimated by the piezoelectric coefficient that describes how the polarization changes in response to stress or strain. We derive two physical quantities, namely the piezoelectric stress coefficient d_{ij} and the piezoelectric strain coefficient (e_{ij}). Specifically, d_{ij} describes the induced polarization in the direction i (ΔP_i) with an applied stress (σ_j), which can be gauged by $\Delta P = d_{ij}\sigma_j$. And e_{ij} links ΔP_i with strain (η_j) given by $\Delta P_i = e_{ij}\eta_j$. Both d_{ij} and e_{ij} are third-rank tensors, and they can be linked via elastic compliances by $d_{ij} = S_{jk}e_{ik}$ [25]. The positive (negative) longitudinal piezoelectric coefficients (e_{33} and d_{33}, assuming the z-axis is the direction of the polar axis) represent a positive (negative) piezoelectric effect. As depicted in figure 1(a), a uniaxial tensile strain increases (decreases) the polarization due to positive (negative) piezoelectric effect [93]. From the perspective of materials, positive piezoelectrics are common. There is an exception, namely the ferroelectric polymerpoly (vinylidene fluoride) (PVDF), which exhibits negative piezoelectric effect [22, 94]. From the perspective of applications, negative piezoelectrics are unique and promising in the devices used for electromechanical systems. As depicted in figure 1(b), the heterostructure constructed by positive and negative piezoelectrics can achieve better ductility.

Recently, more and more quasi-two/one-dimensional ferroelectrics have been reported, and the unique negative piezoelectric mechanisms have also been discovered [93, 77, 95–97]. In this brief review, the negative piezoelectricity in quasi-two/one-dimensional ferroelectrics reported recently will be introduced and categorized.

2. Negative piezoelectricity in low dimensional ferroelectrics

In the following, we review several works on negative piezoelectricity in low dimensional ferroelectrics with different physical mechanisms. The origin of negative piezoelectricity is closely related to that of ferroelectricity. The following examples include vdW layered ferroelectric $CuInP_2S_6$, noncollinear, sliding, and elemental ferroelectrics.

2.1. Giant negative piezoelectricity in $CuInP_2S_6$

2.1.1. Ferroelectricity of $CuInP_2S_6$. The ferroelectricity of $CuInP_2S_6$ (CIPS) has been confirmed experimentally and theoretically, which has attracted intensive attention recently [42–44, 45]. CIPS is one of the vdW layered materials that retains room-temperature ferroelectricity when the thickness is reduced to ∼4 nm, whose structure can be depicted in figures 2(a) and (b). Monolayer of CIPS contain a sulfur framework stuffed with Cu and In ions, and P–P pairs. The bulk system is made up of monolayers assembled by -A-B-A-B- mode along the z-axis, which can be coupled by vdW interaction. The site exchange between the Cu and P–P pair causes two different layers, A and B. The displacement of Cu and other cations converts the space group from $C2/c$ (non-polar) to Cc (polar) with spontaneous out-of-plane polarization.

An important criterion for ferroelectrics is whether the polarization can be switched by an electric field. Piezoresponse force microscopy (PFM) measurements have been used as depicted in figures 2(c) and (d). The butterfly loop of the PFM amplitude signal and the obvious 180° flopping of the phase signal indicate the out-of-plane ferroelectric polarization in CIPS even when the thickness is reduced to ∼4 nm. In addition, second-harmonic generation (SHG) measurements have been used to probe the phase transition from the ferroelectric to paraelectric state in experiments, as shown in figures 2(e) and (f). These experimental results verify the ferroelectricity in few layer CIPS.

2.1.2. Negative piezoelectricity of CIPS confirmed by experiment. Piezoelectricity is a key property associated with ferroelectricity, and it is natural to investigate the piezoelectricity of CIPS [87, 95]. In addition, the anomalous polarization enhancement in CIPS under pressure has been reported by the previous experiment [98]. The converse piezoelectric effect of CIPS is measured by experiment. For comparison, the results of two other prototypical ferroelectric materials are exhibited, *i.e.* PVDF and $Pb(Zr_xTi_{(1-x)})$(PZT) thin films.

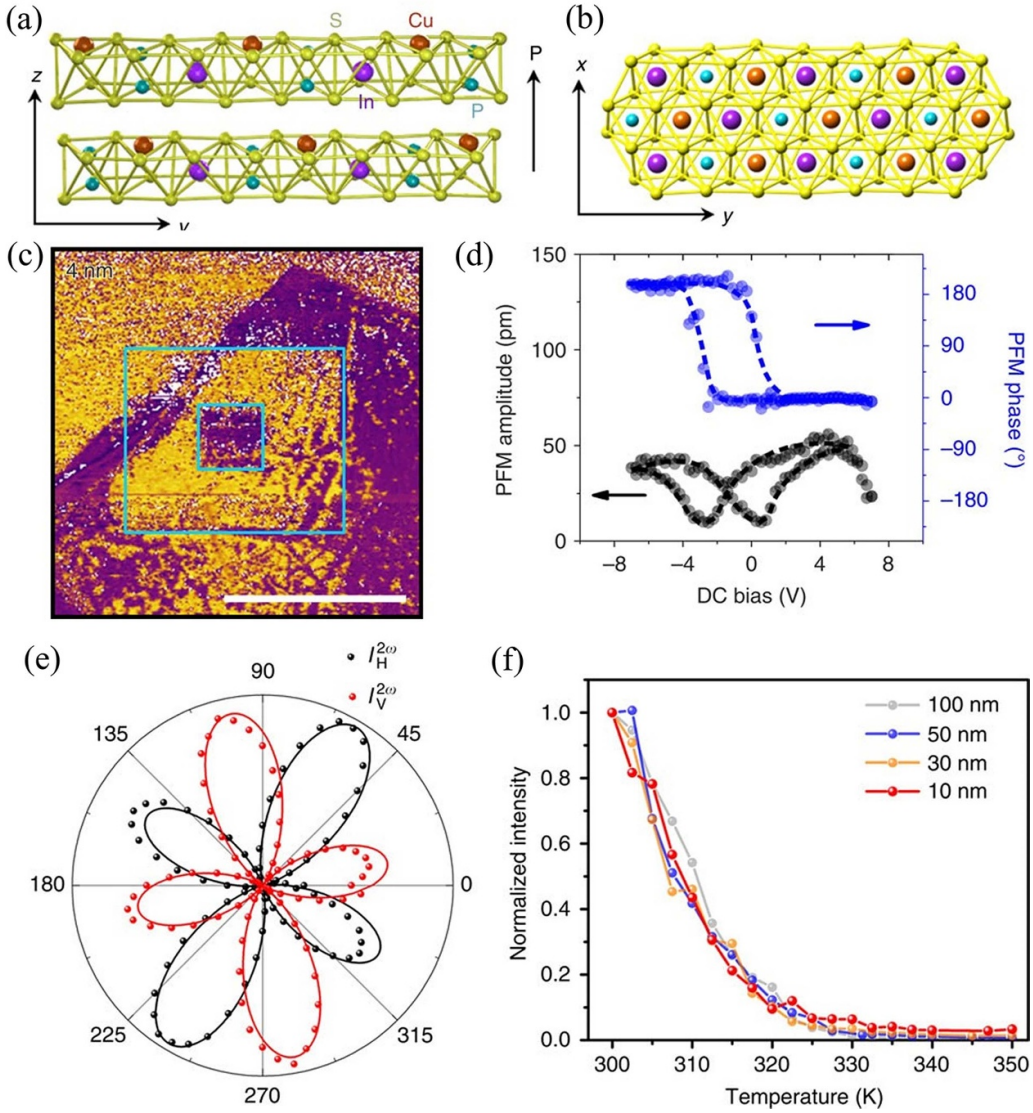

Figure 2. (a) Side view and (b) top view for the structure of bulk CIPS. The arrow indicates the polarization direction. (b) The PFM phase image for 4 nm. (d) The phase (blue) and amplitude (black) hysteresis loop from PFM for 4 nm. (e) SHG intensity in horizontal (H) and vertical (V) directions for a 100 nm. (f) Temperature dependence of SHG intensity with different thickness. Reproduced from [44].

These two materials are known examples of negative piezoelectric and positive piezoelectric, respectively. The polarization, strain and longitudinal piezoelectric coefficient d_{33} as a function of electric field are synchronously recorded as depicted in figure 3.

In the PVDF system, the polarization is downward at the beginning. When the electric field increases from zero to the maximum pointing upward, polarization is switched at the coercive field (E_c). Simultaneously, the strain increases from zero to the peak at the E_c, and flips the symbol after the polarization is completely switched. This phenomenon indicates that the lattice expands (contracts) if the electric field is opposite (same) to the direction of polarization. The electromechanical response of PVDF is consistent with negative piezoelectric effect. On the contrary, the strain–electric field loop for PZT is opposite to PVDF, characterized as the positive piezoelectric effect. While for CIPS, its electromechanical response seems to be similar to PVDF, indicating that it is a negative piezoelectric material.

To double-check this discovery, the piezoelectric coefficients of d_{33} are measured by experiment. PVDF and CIPS show the same behavior, which agrees with the negative piezoelectric effect, while PZT exhibits the positive piezoelectric effect. The effective d_{33} in the zero-field case of PVDF, CIPS, and PZT are about −25, −95, and 48 pm/V, respectively. The large piezoelectric coefficient d_{33} of CIPS indicates a giant negative piezoelectric effect, whose physical mechanism should be revealed.

2.1.3. Phenomenological theory of the negative piezoelectricity in CIPS. The negative piezoelectric effect can be revealed by phenomenological theory. A ferroelectric crystal changes from the paraelectric phase to the polar state, which

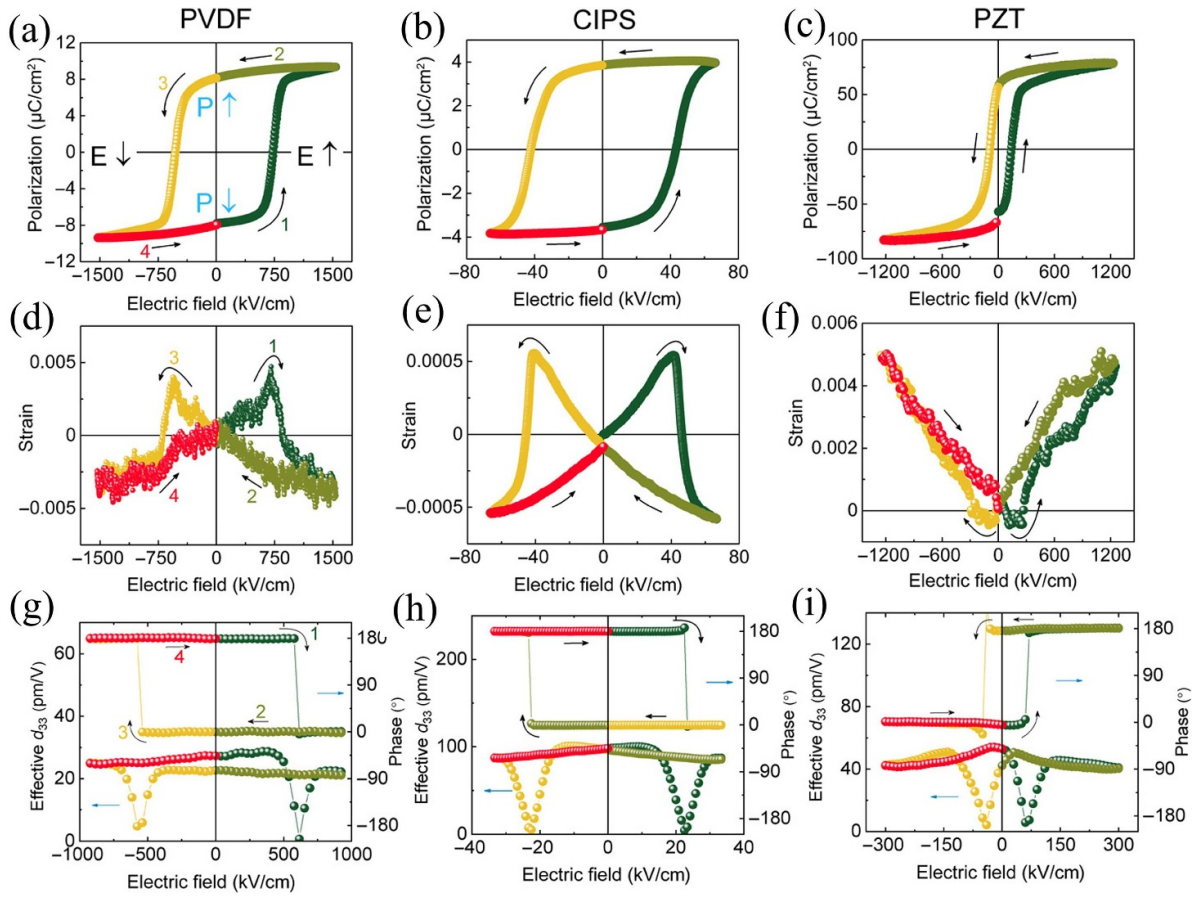

Figure 3. (a)–(c) Polarization-electric field curves for PVDF (a), CIPS (b),and PZT (c). (d)–(f) Corresponding strain-electric loops for PVDF (d), CIPS (e), and PZT (f). (g)–(i) d_{33} of PVDF (g), CIPS (h), and PZT (i), from [95]. Reprinted with permission from AAAS.

can induce the longitudinal strain named as S_{33}. It can be estimated by the Taylor expansion of the electric distortion named as D_3 as shown in the following equation [99]:

$$S_{33} = Q_{33}D_3^2 = Q_{33}\left(\vec{P}_s + \vec{P}_i\right)^2 = Q_{33}\left(\vec{P}_s + \epsilon_{33}\vec{E}_3\right)^2$$
$$= Q_{33}\vec{P}_s{}^2 + 2Q_{33}\epsilon 33\vec{P}_s\vec{E}_3 + Q_{33}\epsilon_{33}^2\vec{E}_3{}^2 \quad (1)$$

where Q_{33} is the coefficient of longitudinal electrostriction, ε_{33} is the dielectric permittivity, $\vec{P}_s$ and $\vec{P}_i$ are the spontaneous and induced polarization. The spontaneous strain induced by the paraelectric-to-ferroelectric phase transition can be described in the first term. The main electromechanical coupling component can be represented by the second term, in other words, piezoelectric coefficient of d_{33} can be defined as $2Q_{33}\epsilon_{33}P_s$. Quadratic electrostriction effect can be shown in the last part [100]. The negative piezoelectricity in ferroelectric systems is the spontaneous negative electrostriction, which can be seen as the expansion of lattice constant along the polar axis when there is a drop of polarization.

2.1.4. Revealing negative piezoelectricity from dimensionality. Unlike perovskite oxide three-dimensional ferroelectrics, the dipole in CIPS exists in isolated layers, which can be stacked together via vdW interaction to form a discontinuous (broken) lattice. The ions and bonds have been simplified to the ball-and-spring model as depicted in figure 4. In PZT, the electric field and polarization are assumed to be along the same direction, and the positive (negative) ions move along (against) the electric field. However, due to the bond anharmonicity of the spontaneous displacement, namely, the compression is harder than the expansion. This results in $\Delta r_1 > \Delta r_2$, and the lattice parameter expands with the enhancement of polarization. Therefore, there is a positive piezoelectricity. However, in CIPS, the isolated dipoles are held together via the vdW interaction, which is very soft. As a result, the elastic compliance of k_4 is very small, resulting in $\Delta r_4 > \Delta r_3$. This means that the lattice parameter shrinks with the enhancement of polarization in CIPS, namely the negative piezoelectricity.

2.1.5. Microscopic origin of negative piezoelectricity in CIPS from computational modeling. Single-crystal x-ray diffraction and first-principles calculations have been performed to reveal the giant negative piezoelectric effect from a microscopic perspective. There are four Cu sites in one of the polarization states, as shown in figure 5(a). In addition, experiment results suggests there is a possible metastable Cu site in the

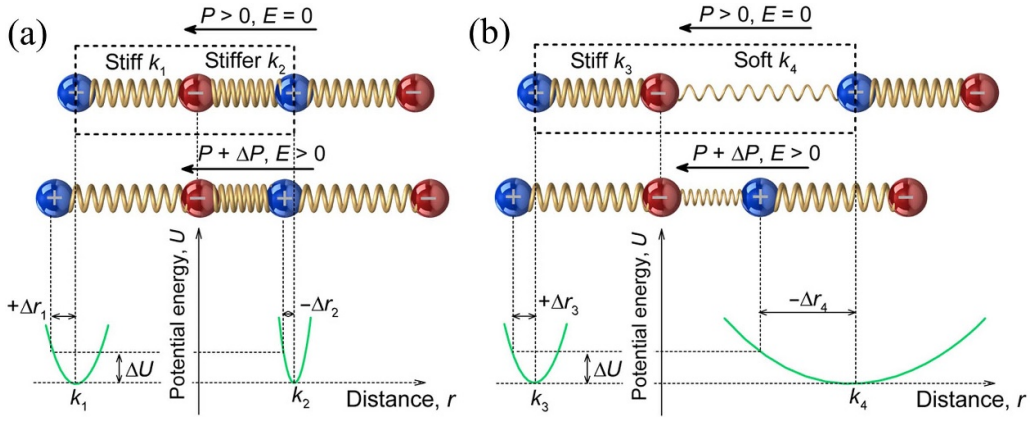

Figure 4. Simplified rigid ion model for piezoelectrics. (a) Positive piezoelectrics with continuous lattice. (b) Negative piezoelectrics with discontinuous lattice. The dashed box indicates the unit cell. The black arrows indicate the directions of polarization and electric field. The pair potential energy profiles of the relevant chemical bonds are shown by the lower parts. From [95]. Reprinted with permission from AAAS.

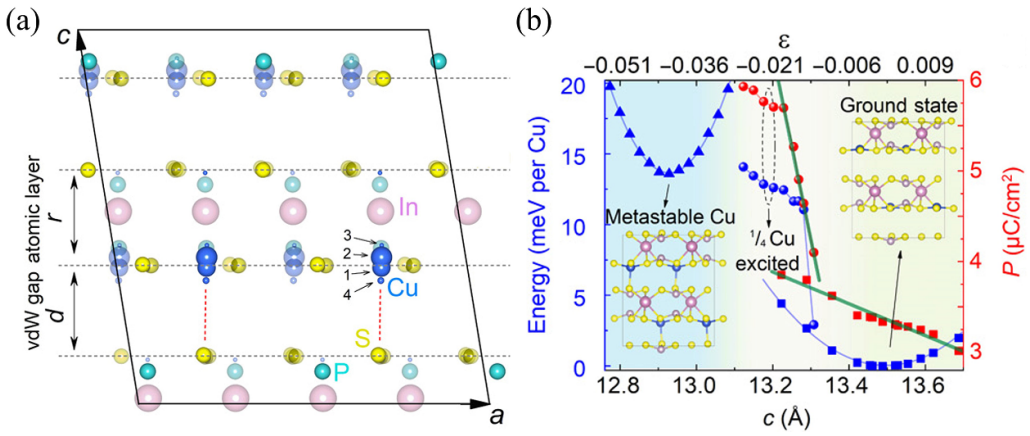

Figure 5. (a) Refined structure of CIPS in unit cell viewed from the *b* axis. The occupation can be indicated by the Cu atoms' size. (b) The free energy *E* (left vertical coordinate) and polarization *P* (right vertical coordinate) changing with lattice constant *c* in different cases: triangle, metastable state occupied by all Cu ions; circle, metastable state occupied by $\frac{1}{4}$ Cu ions; square, ground-state. Insets: the relevant structures. From [95]. Reprinted with permission from AAAS.

vdW gap. The occupancy of the interlayer site is estimated to be 0.08.

From the first-principles calculation, the piezoelectric coefficient d_{33} of the ground state is -18 pC N^{-1}, which is far from the experimental value ($d_{33} \approx -95$ pC N^{-1}). The giant piezoelectricity in CIPS cannot be explained just by the ground state. Then, the partial occupancy is taken into consideration, as depicted in figure 5(b). In addition, taking the occupancy (8%) observed by experiment into consideration, the estimated polarization is $\sim$4.15 μC cm^{-2}, which is consistent with the experimental value. Furthermore, the approximate d_{33} is about -110 pC N^{-1}. The first-principles calculations confirm the shrinking of the distance of vdW layers *d* results in most of the change in *c* lattice constant, while the CIPS layer thickness *r* barely changes, which is consistent with revealing the negative piezoelectricity of dimensionality.

Two important conclusions from the first-principles calculations are presented. First, the shrinking of the vdW layers plays an important role in the negative piezoelectricity of CIPS. Second, the giant magnitude of the piezoelectric coefficient originates from the large displacive instability of the Cu atoms.

2.2. Negative piezoelectricity in noncollinear ferrielectrics

2.2.1. The noncollinear ferrielectricity in monolayer MO_2X_2.

Magnetism and polarity are homotopic according to the Landau theory, which should display the one-to-one correspondence among many physical properties. Examples are ferromagnetic *vs* ferroelectric states and antiferromagnetic *vs* antiferroelectric states. The spin noncollinearity has been widely studied for magnets, while the noncollinear dipole orders are very rare except for a few ferrielectrics, such as three-dimensional materials of $BaFe_2Se_3$ [101], Pb_2MnWO_6 [102], and monolayer MO_2X_2 (*M*: group-VI transition metal; *X*: halogen) [96]. The noncollinear ferrielectricity associated with negative piezoelectricity in monolayer MO_2X_2 will be reviewed in the following.

The paraelectric structure of MO_2X_2 indicates that all *M* ions are located at the center of the O_4X_2 octahedra with the

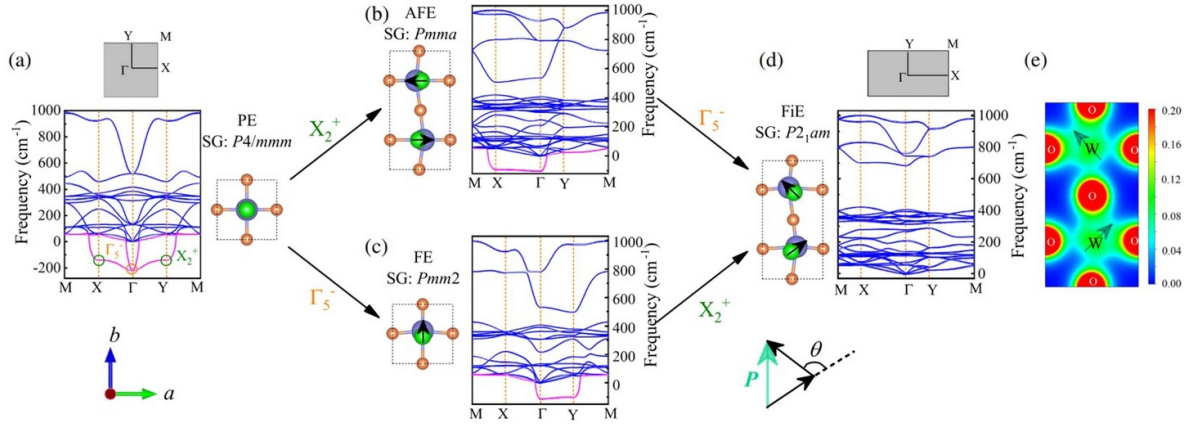

Figure 6. Phonon spectra and structures for different phases of monolayer MO_2X_2. Brillouin zones are represented by the grey squares or rectangles. (a) The paraelectric phase. The imaginary-frequency modes (X_2^+ and Γ_5^-) are indicated. (b) The unstable antiferroelectric state accompanying the distortion mode named X_2^+. (c) The unstable ferroelectric state accompanying the distortion mode named Γ_5^-. (d) The final ferrielectric ground state. The angles marked by θ between nearest neighbor dipoles (black arrows) align the b axis are $\sim$129°. (e) Partial charge density diagram of valence electrons. Reprinted (figure) with permission from [96], Copyright (2019) by the American Physical Society.

space group of $P4/mmm$ (shown in figure 6(a)). The phonon spectrum indicates that the paraelectric structure is unstable with two imaginary-frequency modes, which can result in spontaneous structural distortions. As depicted in figures 6(b) and (c), the unstable mode named X_2^+ at X (and Y) induces antiferroelectric distortions and another unstable mode named Γ_5^- at Γ point results in ferroelectric distortions.

Only one of the phonon modes cannot construct a stable phase. The cooperation of these two modes can lead to a stable phase with a net ferroelectricity (figure 6(d)), whose behavior is similar to the exchange frustration in magnets. The dipole moments at the local sites are noncollinear, and the canting angle of WO_2Cl_2 (MoO_2Br_2) is about 129° (128°) as depicted in the bottom of figure 6. The directions of ferroelectric and antiferroelectric ordering are orthogonal, along the b and a axes. The polarizations along the b-axis of monolayer MoO_2Br_2 and WO_2Cl_2 are estimated to be 32.09 and 26.36 μC cm^{-2} respectively when the distance between adjacent layers is the thickness of the monolayer.

The driving force for polar distortions of these transitional metal oxyhalides should be the d^0 rule from M^{6+}, which means strong coordination bonds can be formed between the empty d orbitals of M ions and $2p$ orbitals of O ions. As shown in figure 6(e), there is a few valence electron transfers from O^{2-} to M^{6+} and this induces ferroelectric distortions.

2.2.2. Negative piezoelectricity induced by the noncollinear ferrielectricity in monolayer MO_2X_2. Different from the plain ferroelectrics, the 180° flipping of the net polarization does not need the 180° switching of all local dipole moments. On the contrary, the collaborative $\sim$50% rotations of the dipole moments on all local sites can also work (figure 7(a)). In addition, the energy barriers induced by the nonpolar transition states for MoO_2Br_2 and WO_2Cl_2 monolayers are 0.399 and 0.158 eV, respectively (figure 7(b)).

Furthermore, the 90° switching of polarization also works, which can be achieved by exchanging the a and b axes. We show that two assuming two-step paths can be seen in figure 7(c). The energy barriers can be depicted in figure 7(d), which induces a slightly lower energy barrier in path II. This unique 90° switching of polarization can further result in the negative piezoelectricity. The reason can be explained as the following. The lattice constants a and b in the orthorhombic ferroelectric phase are unequal, i.e. $a > b$, and the net polarization is along the b-axis. The component of local dipoles along the a-axis is larger than that along the b-axis. Thus, when the net residual polarization undergoes the 90° switching process from the b-axis to a-axis, the lattice constant along the polarization increases, which means that P_a decreases with increasing a (figures 7(e) and (f)) and an anomalous behavior, namely the negative piezoelectricity appears. In other words, the negative piezoelectric effect can be induced by the 90° switching of polarization. However, the specific magnitude of the negative piezoelectric coefficient has not been proven by calculation or experiment, which needs further study.

2.3. Negative piezoelectricity in sliding ferroelectrics

2.3.1. Ferroelectricity in interlayer sliding ferroelectrics. Interlayer sliding ferroelectricity widely exists in two-dimensional vdW materials, which describes the unique phenomenon of the induced ferroelectric polarization perpendicular to the interlayer sliding direction. Sliding ferroelectrics have received extensive experimental and theoretical attention. The origin of sliding ferroelectricity and negative piezoelectricity will be reviewed.

Taking β-ZrI_2 bulk as an example of sliding ferroelectric [77], whose polarization is calculated as 0.39 μC cm^{-2} by first-principles calculations; the polarization direction is along the c-axis. The planar-averaged differential charge density

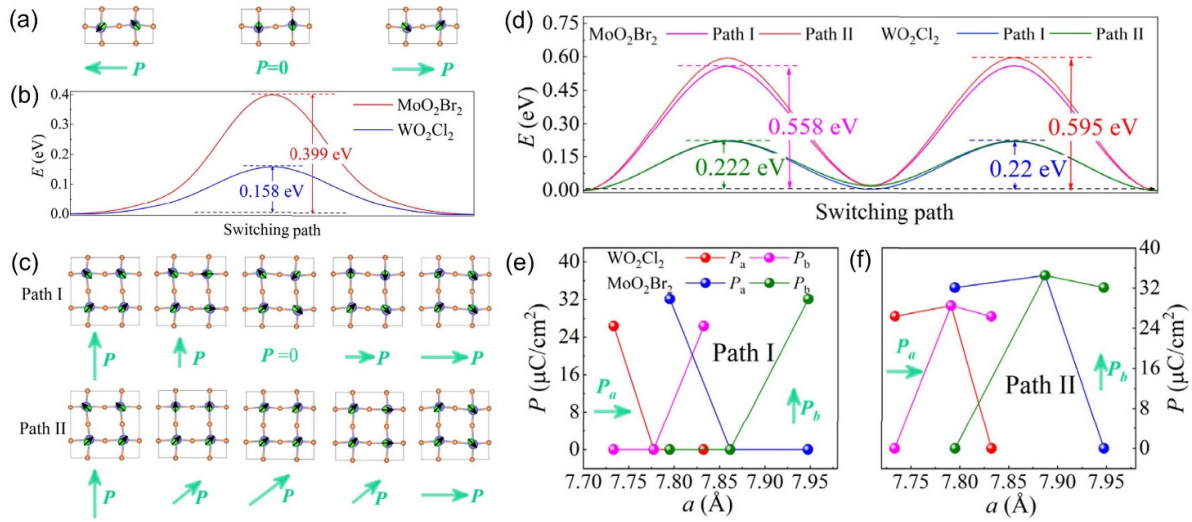

Figure 7. (a) The 180° switching path of the net polarization: ferroelectric-antiferroelectric-ferroelectric. (b) The corresponding energy barriers of the 180° switching of polarization. (c) Two assuming paths (labeled as Path I and Path II) of the 90° switching of polarization by interchanging the a and b axes. (d) The corresponding energy barriers of the 90° switching. (e), (f) The change of local dipoles along the a (P_a) and b (P_b) directions as the function of lattice constant a. The general trend is that P_a reduces with the enlarge of a, namely the negative piezoelectricity. (e) Path I. (f) Path II. Reprinted (figure) with permission from [96], Copyright (2019) by the American Physical Society.

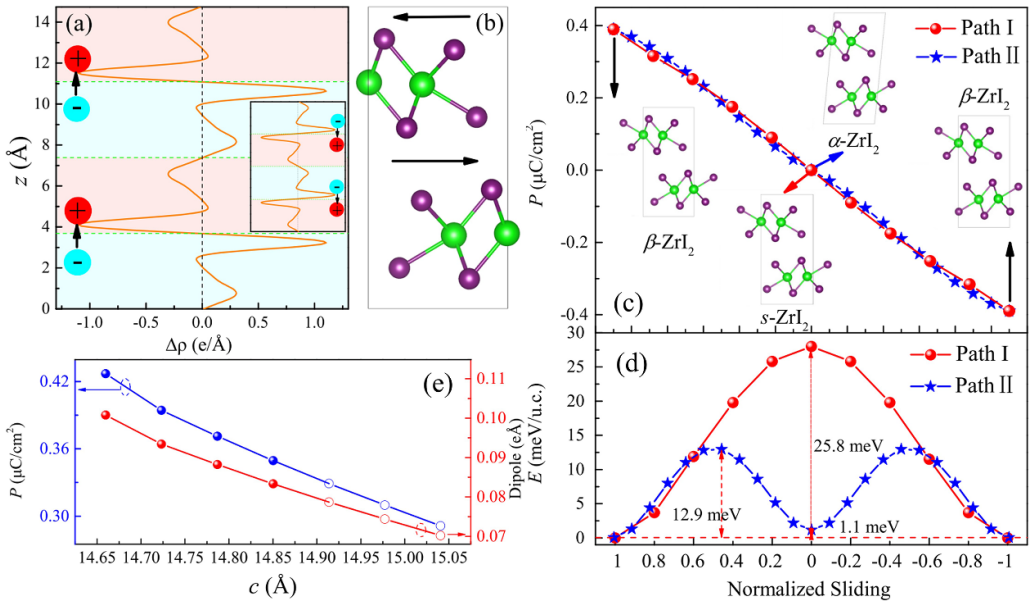

Figure 8. (a) The planar-averaged differential charge density ($\Delta\rho$) projecting along the c-axis, with parent phase (space group: *Pnma*) as the reference. The case of opposite polarization can be shown in the inset. (b) The corresponding structure of (a). (c) Two possible ferroelectric switching paths in β-ZrI_2. (d) The corresponding energy barriers. (e) The polarization and dipole moment of β-ZrI_2 as the function of lattice constant c. Reprinted (figure) with permission from [77], Copyright (2021) by the American Physical Society.

between the ferroelectric and paraelectric (with space group of *Pnma*) has been calculated and can be shown in figure 8(a). It is obvious that there is charge transfer between the upper and lower Zr–I bonds in each layer, which should be induced by the special stacking method with symmetry breaking. In other words, the inequivalent of the chemical environment makes upper Zr–I bonds more charge positive but the lower side more negative and it naturally induces an electric dipole moment in each ZrI_2 layer. Unlike the ZrI_2 bulk, the ZrI_2 bilayer owns both in-plane and out-of-plane polarization. The in-plane polarization can be offset between nearest-neighbor bilayers in the bulk (figure 8(b)).

The direction of polarization can be switched by interlayer sliding. The two ferroelectric switching paths are named as path I and path II as depicted in figure 8(b). Path I is only related to the interlayer sliding among the vdW layers. Path II involves not only interlayer sliding but also changes of the crystallographic axis angle. Both paths can achieve ferroelectric switching but have different energy barriers as depicted figure 8(d).

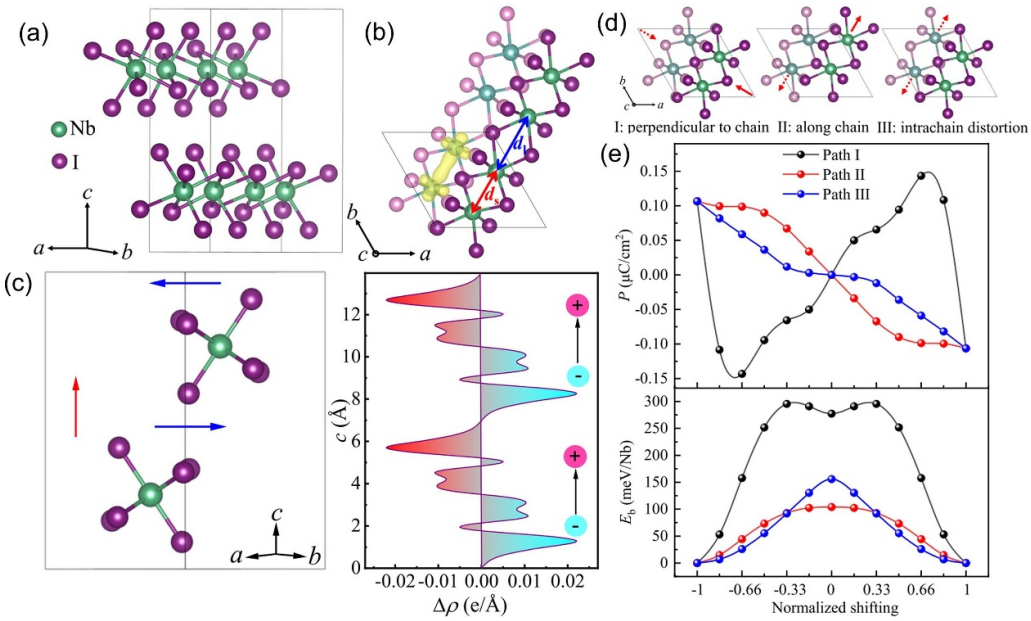

Figure 9. (a) Side view of NbI_4 bulk. Each unit cell contains two chains. (b) View of NbI_4 from the c-axis. The longer d_l and shorter d_s indicate the structural dimerization. (c) Left panel: top view of chains, the blue and red arrows indicate the dipoles. Right panel: The planar-averaged differential electron density $[\Delta\rho = \iint[\rho(+P) - \rho(-P)]\mathrm{d}x\mathrm{d}y]$ along the c-axis. The blue and red arrows indicate p_{ab} and p_c respectively. (d) Three possible ferroelectric switching paths in NbI_4 bulk. (e) Corresponding P and energy barriers for switching paths. Reprinted (figure) with permission from [105], Copyright (2024) by the American Physical Society.

2.3.2. Negative piezoelectricity in sliding ferroelectrics. The polarization can be regulated by the uniaxial stress (changing the lattice constant) aligning the c-axis as depicted in figure 8(e). It is obvious that the polarization increases as the lattice constant decreases, which indicates β-ZrI_2 has the negative piezoelectric effect. Furthermore, the piezoelectric coefficient d_{ij} has been calculated as

$$d_{ij} = \sum_{k=1}^{6} e_{ik} S_{kj} \tag{2}$$

where $S = C^{-1}$ is the elastic compliance coefficient, and C is the elastic tensor. The results show d_{33} is $-1.445\ \mathrm{pC\,N^{-1}}$, which further confirms the negative piezoelectric effect by first-principles calculations.

There are two contributions to the enhancement of polarization accompanying the compression of the lattice constant c. The first term is the decreased volume due to the easily compressible soft vdW layers, which is similar to CIPS [95]. The second term is the increased dipole moment of each unit cell, which is due to the unique origin of interlayer sliding ferroelectricity. Specifically, the closer adjacent ZrI_2 layers, the larger the interlayer sliding, and the greater the vertical polarization. For example, in β-ZrI_2, the contributions of these two parts to negative piezoelectricity are $\sim$5% and $\sim$95%, respectively. In addition, recent reports indicate that the negative piezoelectric effect widely exists in sliding ferroelectrics, including bilayer BN, bilayer WTe_2, 2D Tellurene [65, 66, 103, 104] and quasi-one-dimensional sliding ferroelectric NbI_4 [105].

2.4. Quasi-one-dimensional sliding ferroelectricity and negative piezoelectric effect

There is an obvious advantage of high storage density due to quasi-one-dimensional characteristics, for example, the theoretical upper-limit for ferroelectric memory density can reach $\sim$100 $\mathrm{Tbits\,in^{-2}}$ [106]. Naturally, generalizing the concept of sliding ferroelectricity to quasi-one-dimensional systems is necessary and promising. Recently, the quasi-one-dimensional ferroelectricity in NbI_4 bulk has been reported [105].

Two NbI_4 chains are assembled by vdW force in the primitive cell of NbI_4 bulk. Within each chain, all Nb ions are caged within the I_6 octahedron and the neighboring octahedra are edge-sharing. In addition, the adjacent Nb ions are dimerized as depicted in figures 9(a) and (b). The space group of NbI_4 bulk is $Cmc2_1$, which belongs to the polar point group $mm2$. The polarization can be calculated to $0.11\,\mu\mathrm{C\,cm^{-2}}$, whose direction of polarization is along the c-axis. Similar to the two-dimensional interlayer sliding ferroelectrics, the special binding mode of the isolated two chains can induce perpendicular components (p_c & p_{ab}). Furthermore, the p_c's are parallel between nearest-neighbor pairs, while p_{ab}'s are antiparallel and canceled between nearest-neighbor pairs along the c-axis (Left panel of figure 9(c)). The microscopic origin of the dipoles is the bias of the electron cloud as described in the right panel of figure 9(c).

Unlike interlayer sliding ferroelectrics, there are more degrees of freedom regarding the sliding modes due to the quasi-one-dimensional characteristics of NbI_4. Specifically, we show that three paths can reverse the polarization as depicted in figure 9(d), including sliding along the direction of the

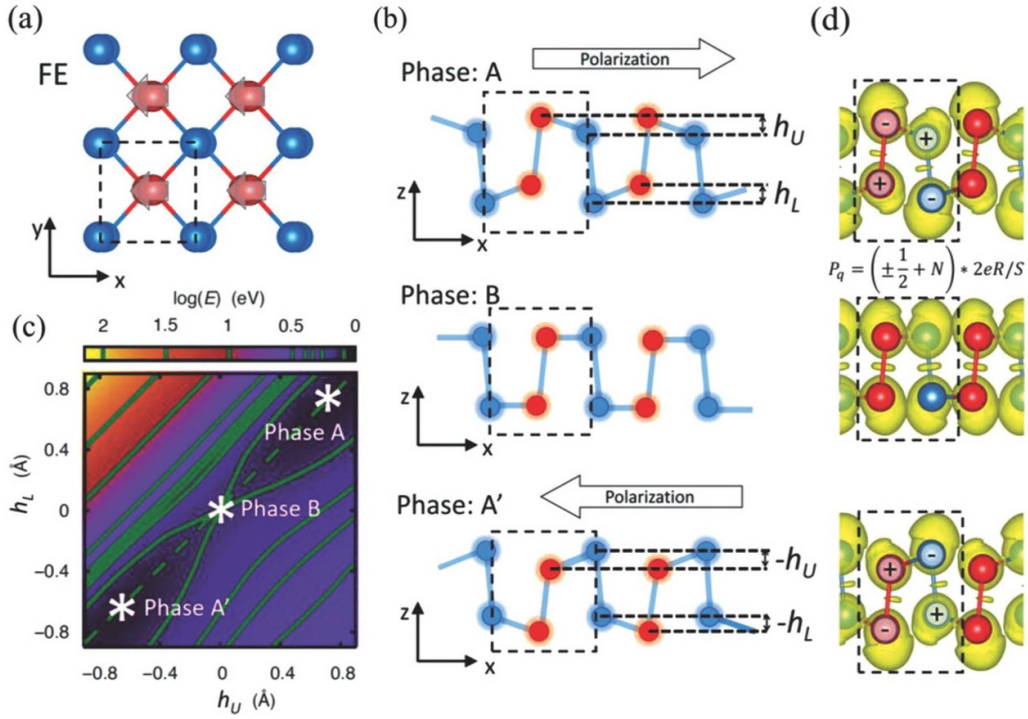

Figure 10. (a) Top view of group-V elemental monolayer. The unit cell is framed by the black dashed rectangle. (b) Side views of ferroelectric states (phases A and A') and paraelectric state (phase (B). (c) Free energy contour for As monolayer as the function of buckling heights (h_U, h_L). (d) The electron localization function for phases A, B, and A'. [53] John Wiley & Sons. [© 2018 WILEY-VCH Verlag GmbH & Co. KGaA, Weinheim].

chain (labeled as I), perpendicular to the chain (labeled as II) and intrachain ion displacements (labeled as III). The corresponding polarization and energy barriers for these three switching paths are shown in figure 9(e). In addition, the negative piezoelectric effect has also been observed in NbI_4 systems with $d_{33} = -0.42$ pC N^{-1}, and the mechanism is similar to that of interlayer sliding ferroelectricity. Namely, the electric dipoles come from interchain couplings, which can be enhanced during volume shrinking. However, the polarization and negative piezoelectric coefficient are very small, which may limit the practical application. Thus, finding systems with better negative piezoelectric properties is one of the research tasks.

2.5. *In-plane negative piezoelectricity in elemental ferroelectrics*

2.5.1. Theoretical prediction of ferroelectricity in elementary ferroelectric monolayers. In recent years, intrinsic two-dimensional ferroelectricity has been discovered for single-element monolayers by first-principles calculations and experiments, which include group-V elements including As, Sb, and Bi [53, 93, 97, 107]. The structure of elemental monolayers is similar to that of buckled black-phosphorene as depicted in figure 10. Due to the partial sp^2 character other than the homogeneous tetrahedral sp^3 hybridization. The space group of the distorted elemental monolayers is $Pmn2_1$, which is the polar group. The buckling can be characterized by two heights labeled h_U and h_L. The structure tends to a phosphorene structure (*Pmna*) with centrosymmetry. There are also two stable energy-degenerate polar phases called phase A and A'. The electron localization function shows the distinct localized lone pair in these two polar states. The polarizations estimated are 46, 75, and 151 pC m^{-1} for monolayer As, Sb, and Bi, respectively. The polarization can be switched through the paraelectric phase B with a moderate energy barrier. Furthermore, the in-plane polarization of the single-element bismuth monolayer has been confirmed by experiment [52].

2.5.2. Large in-plane negative piezoelectricity. Special buckling distortion induces ferroelectricity in single-element materials, which can be significantly affected by external strain. The piezoelectric strain coefficients d_{33} of the two-dimensional elemental-ferroelectrics can be calculated by first-principles calculations, which are -19.2 and -25.9 pC m^{-1} for α-Sb and α-Bi monolayers, respectively. The results indicate a large in-plane negative piezoelectricity in these two-dimensional elemental-ferroelectrics [93].

The mechanism of in-plane negative piezoelectricity in these materials may be tracked back to the origin of ferroelectricity. As mentioned before, the ferroelectric phase with buckling distortion breaks the space inversion symmetry and induces charge asymmetry in the puckered monolayer. From another perspective, the buckling is similar to sliding, which

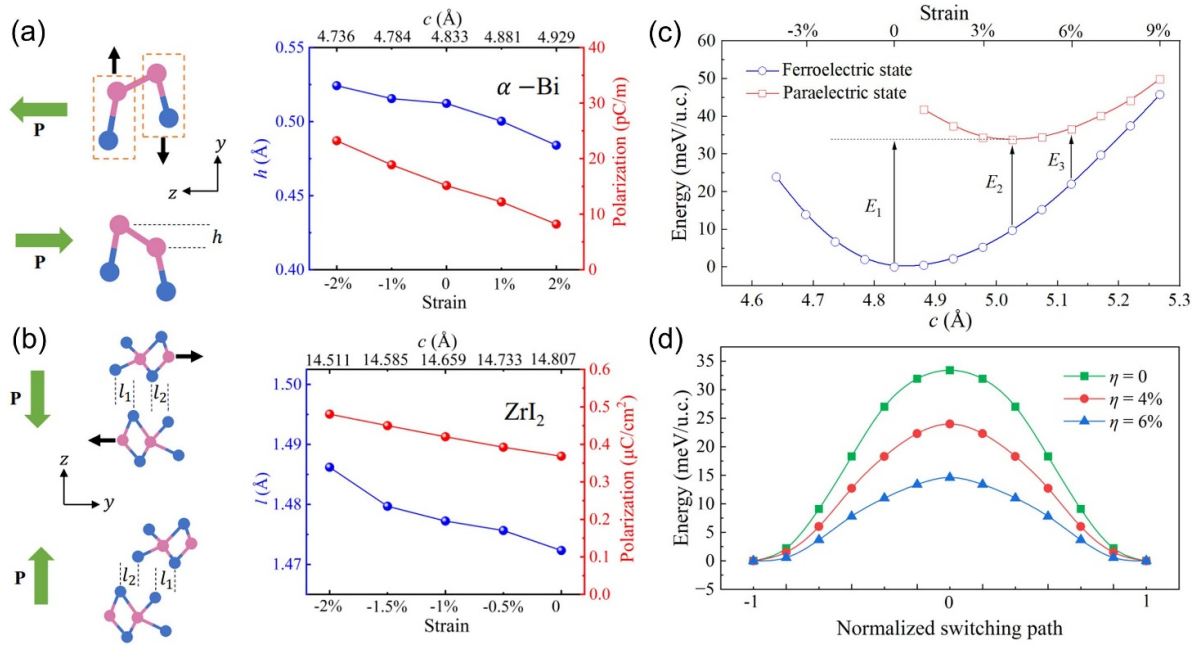

Figure 11. Left panels: the ferroelectric distortion parameters, namely h, $l = l_1+l_2$. l is the sliding distance. The black arrows indicate the directions of atomic movement. Green arrows show the direction of polarization. Right panels: ferroelectric order parameters and polarization as a function of uniaxial strain. (a) Monolayer α-Bi. (b) ZrI_2 bulk. Reprinted (figure) with permission from [93], Copyright (2023) by the American Physical Society.

can be considered as a kind of intercolumn sliding as shown in figures 11(a) and (b). The origin of negative piezoelectricity can be revealed qualitatively. The relative sliding between columns induces a polarization perpendicular to the column direction. The neighboring columns become closer with compressive strain along the direction of the polar axis, and the polarization enhances with greater ferroelectric displacement.

Furthermore, the piezoelectric stress coefficients e_{33} can consist of two terms, namely the clamped-ion part e_{33}^{-} and the internal-strain part e'_{33}. Specifically, e_{33}^{-} indicates the variety of polarization induced by the distortion of lattice with atomic sites fixed, which indicates the effect of electrons' redistribution and the variety of Born effective charge under uniform strain. And e'_{33} is the piezoelectric reply to the structural optimization that emancipates the internal strain, which means that the Born effective charges are fixed. The coefficients of monolayer α-Bi are $e_{33}^{-} = 0.6$, $e'_{33} = -5.7$ in unit of 10^{-10} C m^{-1}. The internal-strain is negative with larger values while the clamped-ion is positive with smaller values. Thus, it is obvious that the negative internal-strain e'_{33} plays the major role in the negative piezoelectricity. This behavior is similar to that of the vdW layered polar material BiTeX [108], but different from the negative piezoelectricity in the three-dimensional ABC ferroelectric [25]. In addition, the negative piezoelectric effect caused by the negative clamped-ion term being larger than the internal strain term can exist in monolayer arsenic chalcogenides and monolayer group IV–V MX_2 [89, 109, 110].

Similar to WO_2X_2 monolayer as mentioned above, a shrunk lattice constant along the polar axis is also discovered in elemental ferroelectrics as an interesting consequence of negative piezoelectricity. As described in figure 11(c), the lattice constant c of paraelectric state is longer than the ferroelectric state, which induces a tensile strain to decrease the energy gain from the ferroelectric displacement. This can reduce the energy loss when the ferroelectric switching process is shown to be in figure 11(d).

2.5.3. Nonanalyticity of piezoelectric response. The nonanalyticity of piezoelectric response is a previously unknown phenomenon, which means that the (negative) piezoelectric coefficients of tensile and compressive strains are different [97]. The origin of this unique property will be explained in detail as follows.

Taking the M_y mirror symmetry of the single-element ferroelectrics into consideration, the internal-strain term $e_{11}^{(i)}$ (same as e_{33} due to the different crystal axes in different papers) can be decomposed into two terms $e_{11,x}^{(i)}$ and $e_{11,z}^{(i)}$. Therefore, the piezoelectric coefficient e_{11} can be wrote as:

$$e_{11} = e_{11}^{(0)} + e_{11,x}^{(i)} + e_{11,z}^{(i)}, \tag{3}$$

where

$$e_{11,x}^{(i)} = \frac{qa}{\Omega}\sum_n Z_{11}^{*}\frac{\partial u_1(n)}{\partial \eta}, e_{11,z}^{(i)} = \frac{qc}{\Omega}\sum_n Z_{13}^{*}\frac{\partial u_3(n)}{\partial \eta}, \tag{4}$$

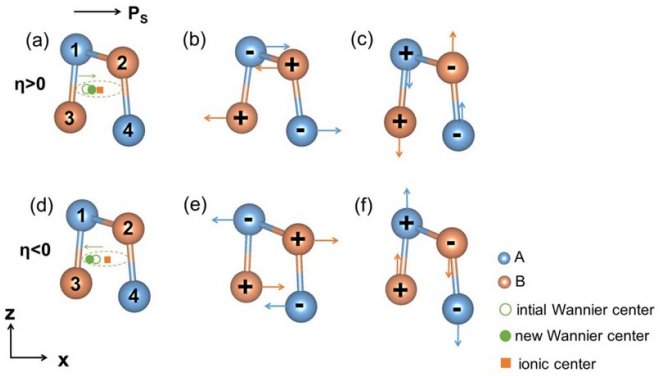

Figure 12. The movements of Wannier center and atomic positions. (a)–(c) $\eta > 0$. (d)–(f) $\eta < 0$. The displacement of Wannier center at the clamped-ion state can be shown by the green dashed oval. The new and initial sites of Wannier center are indicated by the green solid and hollow circle, respectively. The charge center of ions is represented by the orange solid square. The sign of Born effective charges are represented by '+' and '-'. The movement of anions and cations are indicated by the blue and orange arrows. Reprinted (figure) with permission from [97], Copyright (2023) by the American Physical Society.

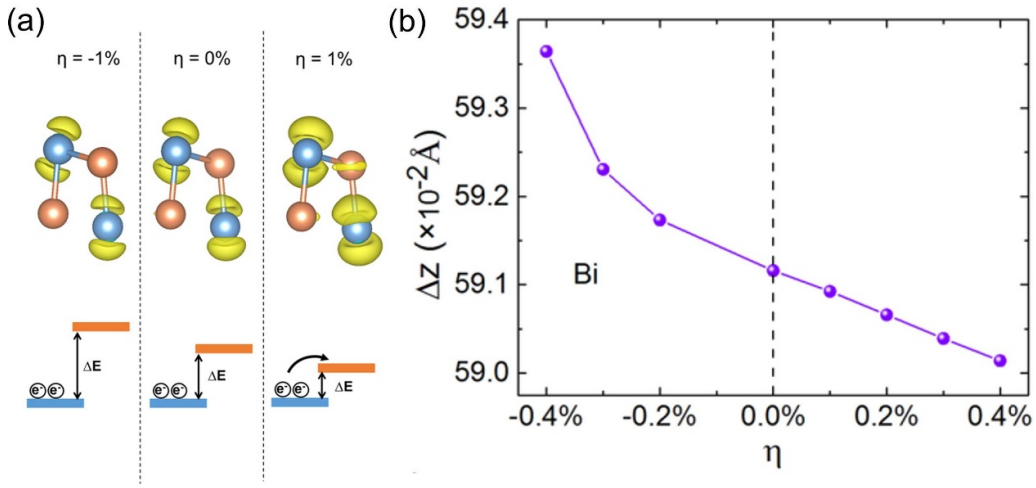

Figure 13. (a) Projected charge densities of p_z orbital for Bi monolayer under different stress conditions. (b) Buckling height Δz with the strain η. Reprinted (figure) with permission from [97], Copyright (2023) by the American Physical Society.

the electron charge is marked by q, a and c are the lattice constants along the x and z axes, Ω and Z^*_{ij} are the area of the unit cell and the Born effective charge, respectively. u_i is the fractional coordinate along i direction.

Both the clamped-ion term and the internal-strain term is negative. First, the negative clamped-ion term indicates 'lag of Wannier center' effect. Specifically, the Wannier center stays away from the center of positive charge and then shifts in the $-x$ direction in the ferroelectric state as depicted by figure 12(a), inducing a polarization along the $+x$ direction ($+P_S$). Imposing a uniform tensile strain $\eta > 0$, Wannier center lags behind and has a relative movement in the direction of polarization, which reduces the net polarization and results in negative $e^{(0)}_{11}$. The second is the negative internal-strain terms $e^{(i)}_{11,x}$ and $e^{(i)}_{11,z}$ are related to the special buckled distortion. There is charge transfer in the ferroelectric state (figure 12(b)), orange and blue sites represent positive and negative charges, respectively. When $\eta > 0$, internal-strain allows the shift of ions along x and z (figures 12(b) and (c)). Two sublattices move toward each other in the x direction, which decreases the polarization P_S. The ions move toward the paraelectric state in the z direction, which also reduces the polarization.

The calculations indicate that in Bi monolayer both the clamped-ion term $e^{(0)}_{11}$ and the internal-strain term $e^{(0)}_{11,z}$ are very different under tensile and compressive strains, but $e^{(0)}_{11,x}$ is almost unchanged [97]. This phenomenon can be named as the nonanalyticity of piezoelectric response, which is closely related to the buckling in Bi monolayer. There is a weak hybridization between 6s and 6p orbitals in the Bi monolayer, and that the p orbitals mainly contribute to the bonds between the Bi atoms. Since the Bi monolayer is extended in the $x-y$ plane, the bonds are mainly determined by p_x and p_y orbitals and p_z electrons form lone pairs, which is the driving force of the buckling (Δz). In addition, the energy difference of p_z levels on the two sublattices acutely affects the distribution of lone-pair electrons, which can be regulated by strain. For small tensile strain, the energy difference of p_z orbitals on the two sublattices can be reduced, which induces charge redistribution and decreases the charge transfer (figure 13(a)). However, for compressive

strain, there is no obvious charge redistribution. The lone-pair electrons also affect the height (Δz). Figure 13(b) indicates Δz under compressive strain changes more rapidly with η, which can explain the nonanalyticity of the piezoelectric response.

3. Summary and outlook

Negative piezoelectric systems not only have common applications in piezoelectric materials but also have unique and promising potential applications in devices used in electromechanical systems. Firstly, piezoelectric materials can produce an electrical voltage in response to an externally mechanical force, which means energy conversion between mechanical energy and the electrical energy can be achieved. Piezoelectric nanogenerators are the main choice to harvest mechanical vibration energy from the surrounding environment, which has been received great attention due to the higher energy density and conversion efficiency [111]. PVDF, a typical negative piezoelectric material, has been widely used in piezoelectric nanogenerator devices [112] including piezo-photodetectors [113, 114], self-powered sensors [115], piezoelectric fibers [116], and triboelectric textile sensors [117]. In addition, the negative piezoelectricity can be an important factor for the output performance of PVDF-based piezoelectric hybrid nanogenerators [118]. Secondly, the negative piezoelectric effect has exclusive and promising potential applications owing to the difference between the response of negative piezoelectric materials to external electric fields and that of positive piezoelectric materials. As depicted in figure 1(b), a heterostructure composed of ultrathin positive piezoelectric and negative piezoelectric layers can be designed when an externally electric field is applied to this heterostructure, then the lattice of normal piezoelectric layers expands but that of the negative piezoelectric layer shrinks. Thus, very large bending in materials can be achieved by constructing the above heterojunctions [93].

In this topical review, the concept of negative piezoelectric effect and the research progress of two-dimensional ferroelectrics were introduced. Furthermore, the negative piezoelectricity in quasi-two/one-dimensional ferroelectrics reported in recent works was reviewed case by case. The mechanisms of negative piezoelectricity are highly different, which are closely related to the origin of ferroelectricity. It can be roughly categorized into the following four types. First, in the CIPS system, the soft vdW layer is responsible for the volume shrinking upon pressure while the electric dipoles are from the non vdW layer. Second, the negative piezoelectricity in two-dimensional MO_2X_2 is due to the noncollinearity of local dipoles, which results in the orthogonal ferroelectric and antiferroelectric axes. Third, the origin of negative piezoelectricity in interlayer/quasi-one-dimensional sliding ferroelectrics are the joint contribution of dipole moment increase and volume decrease. Fourth, the large in-plane negative piezoelectricity in monolayer Bi is highly related to the buckling structure.

Research on piezoelectric properties in low-dimensional ferroelectrics is in the ascendant, and experience can be learned from perovskite systems. Previous studies indicate that the high piezoelectricity in traditional ferroelectrics including $Pb(Zr,Ti)O_3$ (PZT) [119], $Pb(Mg_{1/3}Nb_{2/3}O_3)$-$PbTiO_3$ (PMN-PT) [120] and Sm-doped PMN-PT system [121–123] benefits from the morphotropic phase boundary (MPB) and nanoscale structural heterogeneity [121]. Although some works have focussed on MPB in the low-dimensional ferroelectrics [48, 91, 92], achieving phase coexistence and designing possible polarization rotation are still a challenges for vdW ferroelectrics. Whether a giant negative piezoelectric effect in low-dimensional ferroelectrics can be obtained through MPB remains to be further studied. In addition, previous work has reported that a highly polarizable ionic-covalent matrix benefits from the giant piezoelectricity in a non-MPB ferroelectric $x\mathrm{Bi}(\mathrm{Ni}_{0.5}\mathrm{Hf}_{0.5})\mathrm{O}_3$-$(1\text{-}x)\mathrm{PbTiO}_3$, which has been revealed by techniques such as neutron pair distribution functions and complementary Raman scattering measurements [124]. In addition, domain switching and lattice strain are important processes contributing to the large electromechanical response of perovskite-based piezoelectrics, and the coupling between them has also been reported in previous works [125, 126]. These research experiences can be used as a reference in the study of two-dimensional piezoelectric materials.

With the exception of CIPS and the two-dimensional ferroelectric metal distorted MoS_2 [127] reported by recent experiments, these studies of the negative piezoelectric effect are mainly performed by first-principles calculations. In other words, there are still very few negative piezoelectrics that have been experimentally verified, which requires further exploration. In addition, the mechanisms of negative piezoelectric effect should be more diverse with the increasing number of discoveries of low-dimensional ferroelectric materials. Finally, device design related to the negative piezoelectric effect in low-dimensional ferroelectrics is lacking, which will open a new scientific era.

Data availability statement

No new data were created or analysed in this study.

Acknowledgments

We thank Prof. Junling Wang, Prof. Lu You, Dr Ling-Fang Lin, Dr Yang Zhang, Haoshen Ye, and Ziwen Wang for helpful discussions. This work was supported by the National Natural Science Foundation of China (Grant Nos. 12325401, 12274069), Jiangsu Funding Program for Excellent Postdoctoral Talent under Grant Number 2024ZB001 and China Postdoctoral Science Foundation under Grant Number 2024M760423.

ORCID iD

Shuai Dong https://orcid.org/0000-0002-6910-6319

References

[1] Jiang A Q, Wang C, Jin K J, Liu X B, Scott J F, Hwang C S, Tang T A, Lu H B and Yang G Z 2011 *Adv. Mater.* **23** 1277–81
[2] Naber R C, Asadi K, Blom P W, De Leeuw D M and De Boer B 2010 *Adv. Mater.* **22** 933–45
[3] Ahn C, Rabe K and Triscone J M 2004 *Science* **303** 488–91
[4] Waghmare U, Spaldin N, Kandpal H and Seshadri R 2003 *Phys. Rev.* B **67** 125111
[5] Tanisaki S 1963 *J. Phys. Soc. Japan* **18** 1181–91
[6] Tokunaga M and Matsubara T 1966 *Prog. Theor. Phys.* **35** 581–99
[7] Lin L F, Xu Q R, Zhang Y, Zhang J J, Liang Y P and Dong S 2017 *Phys. Rev. Mater.* **1** 071401
[8] Hill N A 2000 *J. Phys. Chem.* B **104** 6694–709
[9] Scott J F 2007 *Science* **315** 954–9
[10] Scott J F and de Araujo C A P 1989 *Science* **246** 1400–5
[11] Varghese J, Whatmore R W and Holmes J D 2013 *J. Mater. Chem.* C **1** 2618–38
[12] Martin L W and Rappe A M 2016 *Nat. Rev. Mater.* **2** 16087
[13] Wooten E L *et al* 2000 *IEEE J. Sel. Top. Quantum* **6** 69–82
[14] Muralt P 2000 *J. Micromech. Microeng.* **10** 136
[15] Fu H and Cohen R E 2000 *Nature* **403** 281–3
[16] Saito Y, Takao H, Tani T, Nonoyama T, Takatori K, Homma T, Nagaya T and Nakamura M 2004 *Nature* **432** 84–87
[17] Wang Z L and Song J 2006 *Science* **312** 242–6
[18] Ahart M, Somayazulu M, Cohen R E, Ganesh P, Dera P, Mao H K, Hemley R J, Ren Y, Liermann P and Wu Z 2008 *Nature* **451** 545–8
[19] Setter N *et al* 2006 *J. Appl. Phys.* **100** 051606
[20] Mao Y, Zhao P, McConohy G, Yang H, Tong Y and Wang X 2014 *Adv. Energy Mater.* **4** 1301624
[21] Thomann H 1990 *Adv. Mater* **2** 458–63
[22] Katsouras I *et al* 2016 *Nat. Mater.* **15** 78–84
[23] Bernardini F, Fiorentini V and Vanderbilt D 1997 *Phys. Rev.* B **56** R10024
[24] Shimada K 2006 *Jpn. J. Appl. Phys.* **45** L358
[25] Liu S and Cohen R 2017 *Phys. Rev. Lett.* **119** 207601
[26] Novoselov K S, Geim A K, Morozov S V, Jiang D e, Zhang Y, Dubonos S V, Grigorieva I V and Firsov A A 2004 *Science* **306** 666–9
[27] Chhowalla M, Liu Z and Zhang H 2015 *Chem. Soc. Rev.* **44** 2584–6
[28] Lin Y, Williams T V and Connell J W 2010 *J. Phys. Chem. Lett.* **1** 277–83
[29] Wang C, You L, Cobden D and Wang J 2023 *Nat. Mater.* **22** 542–52
[30] Zhang D, Schoenherr P, Sharma P and Seidel J 2023 *Nat. Rev. Mater.* **8** 25–40
[31] Wu M and Jena P 2018 *WIREs Comput. Mol. Sci.* **8** e1365
[32] Guan Z, Hu H, Shen X, Xiang P, Zhong N, Chu J and Duan C 2020 *Adv. Electron. Mater.* **6** 1900818
[33] Qi L, Ruan S and Zeng Y J 2021 *Adv. Mater.* **33** 2005098
[34] Wu M, Burton J, Tsymbal E Y, Zeng X C and Jena P 2012 *J. Am. Chem. Soc.* **134** 14423–9
[35] Wu M, Burton J D, Tsymbal E Y, Zeng X C and Jena P 2013 *Phys. Rev.* B **87** 081406
[36] Kan E, Wu F, Deng K and Tang W 2013 *Appl. Phys. Lett.* **103** 193103
[37] Jiang S, Arguilla M Q, Cultrara N D and Goldberger J E 2015 *Acc. Chem. Res.* **48** 144–51
[38] Sainsbury T, Satti A, May P, Wang Z, McGovern I, Gun'ko Y K and Coleman J 2012 *J. Am. Chem. Soc.* **134** 18758–71
[39] Voiry D, Goswami A, Kappera R, e Silva Cde C, Kaplan D, Fujita T, Chen M, Asefa T and Chhowalla M 2015 *Nat. Chem.* **7** 45–49
[40] Zhou L, He B, Yang Y and He Y 2014 *RSC Adv.* **4** 32570–8
[41] Shirodkar S N and Waghmare U V 2014 *Phys. Rev. Lett.* **112** 157601
[42] Belianinov A, He Q, Dziaugys A, Maksymovych P, Eliseev E, Borisevich A, Morozovska A, Banys J, Vysochanskii Y and Kalinin S V 2015 *Nano Lett.* **15** 3808–14
[43] Chyasnavichyus M, Susner M A, Ievlev A V, Eliseev E A, Kalinin S V, Balke N, Morozovska A N, McGuire M A and Maksymovych P 2016 *Appl. Phys. Lett.* **109** 172901
[44] Liu F *et al* 2016 *Nat. Commun.* **7** 12357
[45] Brehm J A *et al* 2020 *Nat. Mater.* **19** 43–48
[46] Chang K *et al* 2016 *Science* **353** 274–8
[47] Fei R, Kang W and Yang L 2016 *Phys. Rev. Lett.* **117** 097601
[48] Song S, Zhang Y, Guan J and Dong S 2021 *Phys. Rev.* B **103** L140104
[49] Ding W, Zhu J, Wang Z, Gao Y, Xiao D, Gu Y, Zhang Z and Zhu W 2017 *Nat. Commun.* **8** 14956
[50] Zhou Y *et al* 2017 *Nano Lett.* **17** 5508–13
[51] Xue F *et al* 2018 *ACS Nano* **12** 4976–83
[52] Gou J, Bai H, Zhang X, Huang Y L, Duan S, Ariando A, Yang S A, Chen L, Lu Y and Wee A T S 2023 *Nature* **617** 67–72
[53] Xiao C, Wang F, Yang S A, Lu Y, Feng Y and Zhang S 2018 *Adv. Funct. Mater.* **28** 1707383
[54] Bruyer E, Di Sante D, Barone P, Stroppa A, Whangbo M H and Picozzi S 2016 *Phys. Rev.* B **94** 195402
[55] Xu B, Xiang H, Xia Y, Jiang K, Wan X, He J, Yin J and Liu Z 2017 *Nanoscale* **9** 8427–34
[56] Zhang S H and Liu B G 2018 *Nanoscale* **10** 5990–6
[57] Zhang J J, Guan J, Dong S and Yakobson B I 2019 *J. Am. Chem. Soc.* **141** 15040–5
[58] Sun W, Ding N, Chen J, You H P, Peng J, Wang S S and Dong S 2022 *Phys. Rev. Mater.* **6** 104404
[59] Song S, Gui C, Dong S, Liu D and Guan J 2024 *J. Mater. Chem.* C **12** 6487–94
[60] Yang C *et al* 2021 *ACS Appl. Mater. Interfaces* **13** 13517–23
[61] Wang Z, Ding N, Gui C, Wang S S, An M and Dong S 2021 *Phys. Rev. Mater.* **5** 074408
[62] Li L and Wu M 2017 *ACS Nano* **11** 6382–8
[63] Yasuda K, Wang X, Watanabe K, Taniguchi T and Jarillo-Herrero P 2021 *Science* **372** 1458–62
[64] Vizner Stern M, Waschitz Y, Cao W, Nevo I, Watanabe K, Taniguchi T, Sela E, Urbakh M, Hod O and Ben Shalom M 2021 *Science* **372** 1462–6
[65] Yang Q, Wu M and Li J 2018 *J. Phys. Chem. Lett.* **9** 7160–4
[66] Liu X, Yang Y, Hu T, Zhao G, Chen C and Ren W 2019 *Nanoscale* **11** 18575–81
[67] Fei Z, Zhao W, Palomaki T A, Sun B, Miller M K, Zhao Z, Yan J, Xu X and Cobden D H 2018 *Nature* **560** 336–9
[68] Sharma P, Xiang F X, Shao D F, Zhang D, Tsymbal E Y, Hamilton A R and Seidel J 2019 *Sci. Adv.* **5** eaax5080
[69] Xiao J *et al* 2020 *Nat. Phys.* **16** 1028–34
[70] Wang X, Yasuda K, Zhang Y, Liu S, Watanabe K, Taniguchi T, Hone J, Fu L and Jarillo-Herrero P 2022 *Nat. Nanotechnol.* **17** 367–71
[71] Wan Y *et al* 2022 *Phys. Rev. Lett.* **128** 067601
[72] Sui F, Jin M, Zhang Y, Qi R, Wu Y N, Huang R, Yue F and Chu J 2023 *Nat. Commun* **14** 36
[73] Miao L P, Ding N, Wang N, Shi C, Ye H Y, Li L, Yao Y F, Dong S and Zhang Y 2022 *Nat. Mater.* **21** 1158–64

[74] Liu X, Pyatakov A P and Ren W 2020 *Phys. Rev. Lett.* **125** 247601
[75] Zhang T, Liang Y, Xu X, Huang B, Dai Y and Ma Y 2021 *Phys. Rev.* B **103** 165420
[76] Ma X, Liu C, Ren W and Nikolaev S A 2021 *npj Comput. Mater.* **7** 177
[77] Ding N, Chen J, Gui C, You H, Yao X and Dong S 2021 *Phys. Rev. Mater.* **5** 084405
[78] Chen X, Ding X, Gou G and Zeng X C 2024 *Nano Lett.* **24** 3089–96
[79] Meng P *et al* 2022 *Nat. Commun.* **13** 7696
[80] Liu K, Ma X, Xu S, Li Y and Zhao M 2023 *npj Comput. Mater.* **9** 16
[81] Yang L, Ding S, Gao J and Wu M 2023 *Phys. Rev. Lett.* **131** 096801
[82] Liang Y, Mao N, Dai Y, Kou L, Huang B and Ma Y 2021 *npj Comput. Mater.* **7** 172
[83] Xiao R C, Gao Y, Jiang H, Gan W, Zhang C and Li H 2022 *npj Comput. Mater.* **8** 138
[84] Zhou J 2022 *npj 2D Mater. Appl.* **6** 15
[85] Wu M and Li J 2021 *Proc. Natl Acad. Sci.* **118** e2115703118
[86] Ji J, Yu G, Xu C and Xiang H J 2023 *Phys. Rev. Lett.* **130** 146801
[87] Qi Y and Rappe A M 2021 *Phys. Rev. Lett.* **126** 217601
[88] Cui Y, Wang T, Hu D, Wang Z, Hong J and Wang X 2024 *npj 2D Mater. Appl.* **8** 62
[89] Zhao Y, Gou G, Lu X and Hao Y 2021 *J. Mater. Chem.* C **9** 6068–77
[90] Fei R, Li W, Li J and Yang L 2015 *Appl. Phys. Lett.* **107** 173104
[91] Deng J *et al* 2024 *2D Mater.* **11** 035034
[92] Wang Y and Wu M 2024 *Nano Lett.* **24** 9868–73
[93] Wang Z and Dong S 2023 *Phys. Rev.* B **108** 235423
[94] Bystrov V S, Paramonova E V, Bdikin I K, Bystrova A V, Pullar R C and Kholkin A L 2013 *J. Mol. Model.* **19** 3591–602
[95] You L *et al* 2019 *Sci. Adv.* **5** eaav3780
[96] Lin L F, Zhang Y, Moreo A, Dagotto E and Dong S 2019 *Phys. Rev. Lett.* **123** 067601
[97] Zhong S, Zhang X, Liu S, Yang S A and Lu Y 2023 *Phys. Rev. Lett.* **131** 236801
[98] Yao X *et al* 2023 *Nat. Commun.* **14** 4301
[99] Lines M E and Glass A M 2001 *Principles and Applications of Ferroelectrics and Related Materials* (Oxford University Press)
[100] Li F, Jin L, Xu Z and Zhang S 2014 *Appl. Phys. Rev.* **1** 011103
[101] Dong S, Liu J M and Dagotto E 2014 *Phys. Rev. Lett.* **113** 187204
[102] Orlandi F, Righi L, Cabassi R, Delmonte D, Pernechele C, Bolzoni F, Mezzadri F, Solzi M, Merlini M and Calestani G 2014 *Inorg. Chem.* **53** 10283–90
[103] Jiang W *et al* 2022 *Phys. Rev.* B **106** 054104
[104] Sachdeva P K, Gupta S and Bera C 2024 *J. Phys.: Condens. Matter* **36** 215701
[105] Ding N, Ye H and Dong S 2024 *Phys. Rev.* B **110** 024115
[106] Lin L F, Zhang Y, Moreo A, Dagotto E and Dong S 2019 *Phys. Rev. Mater.* **3** 111401(R)
[107] Hong Y, Deng J, Kong Q, Yin Y, Ding X, Sun J and Liu J Z 2024 *Phys. Rev.* B **109** 035204
[108] Kim J, Rabe K M and Vanderbilt D 2019 *Phys. Rev.* B **100** 104115
[109] Gao W and Chelikowsky J R 2020 *Nano Lett.* **20** 8346–52
[110] Xu Y, Li Z, He C, Li J, Ouyang T, Zhang C, Tang C and Zhong J 2020 *Appl. Phys. Lett.* **116** 023103
[111] Liu H, Zhong J, Lee C, Lee S W and Lin L 2018 *Appl. Phys. Rev.* **5** 041306
[112] Chang C, Tran V H, Wang J, Fuh Y K and Lin L 2010 *Nano Lett.* **10** 726–31
[113] Si S K, Paria S, Karan S K, Ojha S, Das A K, Maitra A, Bera A, Halder L, De A and Khatua B B 2020 *Nanoscale* **12** 7214–30
[114] Bhattacharya D, Bayan S, Mitra R K and Ray S K 2021 *Nanoscale* **13** 15819–29
[115] Li H, Song H, Long M, Saeed G and Lim S 2021 *Nanoscale* **13** 2542–55
[116] Scheffler S and Poulin P 2022 *ACS Appl. Mater. Interfaces* **14** 16961–82
[117] Lee J E, Shin Y E, Lee G H, Kim J, Ko H and Chae H G 2021 *Composites* B **223** 109098
[118] Guo H, Li L, Wang F, Kim S W and Sun H 2022 *ACS Appl. Mater. Interfaces* **14** 34733–41
[119] Service R F 1997 *Science* **275** 1878–1878
[120] Park S E and Shrout T R 1997 *J. Appl. Phys.* **82** 1804–11
[121] Li F *et al* 2019 *Science* **364** 264–8
[122] Li F *et al* 2018 *Nat. Mater.* **17** 349–54
[123] Kumar N, Mishra A, De A, Shankar U and Ranjan R 2020 *J. Appl. Phys.* **53** 165302
[124] Datta K, Kumar N, Upadhyay A, Mihailova B and Ranjan R 2021 *Phys. Rev.* B **104** L140104
[125] Hall D A, Steuwer A, Cherdhirunkorn B, Mori T and Withers P J 2004 *J. Appl. Phys.* **96** 4245–52
[126] Kumar N, Khatua D K, Mahale B and Ranjan R 2018 *Phys. Rev.* B **97** 134113
[127] Lu H, Aramberri H, Lipatov A, Proksch R, Sinitskii A, Íñiguez J and Gruverman A 2023 *ACS Mater. Lett.* **5** 3136–41